Atlantis Highlights in Engineering, volume 8
Proceedings of the International Renewable Energy Storage Conference 2021 (IRES 2021)

An Open Circuit Voltage and Overpotential Model for an All Vanadium Redox Flow Battery Derived from Several Years of Operating Data

Christoph Stegner*
Energy Storage
ZAE Bayern
Hof, Germany
christoph.stegner@zae-bayern.de

***Abstract*—One essential part in the simulation of electrochemical storage systems like redox flow batteries is the voltage on cell level. In this study, a model is derived for the open circuit voltage and the overpotentials of an all Vanadium system, based on the operation data of three commercial batteries over an extended period. The high amount of observations, especially the combination of a wide range of electrolyte temperatures and currents at different states of charge, allows for the correct identification and modelling of the relations between voltage and the measured variables. Different variants of Nernst equations are evaluated and it is found that considering temperature dependent standard electrode potentials and the inclusion of proton concentration in the catholyte are vital. Three types of overpotentials are modelled and respective parameters defining mass and charge transport are derived from the experimental data.**

Keywords—all Vanadium redox flow, electrochemical storage, simulation, voltage model, open circuit voltage, overpotential

I. Introduction

The all Vanadium redox flow battery (VRFB) is probably the most commercially established variant of flow batteries. Its complex setup requires taking into account electrochemical, thermal, hydraulic and mechanical aspects, amongst others. Studies on the theory and simulation of VRFB are numerous and in the best case based on experiments, like [2],[3],[8],[9],[13],[16] to name a few. In this study, the focus lies on the voltage of a VRFB, which is the sum of the open circuit voltage (OCV) and overpotentials. The source of the data are not experimental runs in the laboratory but the operation of three commercial systems with 30 kW and 130 kWh nominal power and capacity each, that have been running for several years.

II. Method

A. Equipment

The batteries evaluated are three identical, commercial systems with a nominal power and capacity of 30 kW and 130 kWh. Since their commissioning the batteries had undergone different operating histories, leading to different charge cycles, standby times and consequently different aging, before reaching the time span of which measurements for this study are taken from. One battery consists of 20 stacks containing 20 cells each. Two stacks are electrically connected in series forming ten parallel strings per battery. Considering the flow of catholyte and anolyte each half-cell is supplied with its respective electrolyte via parallel inlets.

B. Data

The data used was measured during the operation of the three VRFB in the years 2016 to 2020. No additional measuring equipment was implemented. Instead, the manufacturer made measurements of the built-in sensors available through Modbus-TCP. Measurement includes individual DC current and voltage for every stack, OCV of a reference cell, electrolyte temperature and the power consumption of the electrolyte pumps. The analysis will not be based on single time series but on the entirety of the measure data over a certain period and can best be considered as a cloud of quasi-steady state observations – defined by partial load, temperature, state of charge (SOC), etc. The high granularity of the measure data, regarding both time (5 s intervals) and number of stacks (60), thus grants a degree of statistical significance when used in fitting algorithms.

C. Theory

1) Vanadium Redox Reactions and Concentrations

The following two half-reactions take place during the charge of the VRFB at the positive electrode (1) or cathode

(C) and the negative electrode (2) or anode (A) and occur in reverse direction when discharging:

$$VO^{2+} + H_2O \rightarrow VO_2^{+} + e^{-} + 2\,H^{+} \quad | E^0_{C,ref} = 1.001\ V \quad (1)$$

$$V^{3+} + e^{-} \rightarrow V^{2+} \quad | E^0_{A,ref} = -0.255\ V \quad (2)$$

where $E^0_{C,ref}$ and $E^0_{A,ref}$ are the standard electrode potentials relative to the standard hydrogen electrode at reference temperature 298.15 K according to [4]. Both tanks, the one supplying the cathodes and the other one supplying the anodes, were filled with the same raw electrolyte before the operation of the VRFB. In this raw condition half of the Vanadium ions exist in oxidation state +IV (VO^{2+} or *V4* in this study) the other half as +III (V^{3+} or *V3*). Pre-charging leads to pure *V4* concentration in the catholyte and pure *V3* in the anolyte. This conditions is defined as fully discharged or a SOC of zero. When all Vanadium transformed to oxidation state +V (VO_2^{+} or *V5*) in the catholyte and, by association, to +II (V^{2+} or *V2*) in the anolyte, the battery is fully charged at a SOC of 100 %.

2) Open Circuit Voltage

The open circuit voltage E_{OCV} of a VRFB cell can be calculated using the Nernst equation, which describes the difference of the electrode potential E^0 of the vanadium redox pair. Activity coefficients can be assumed ideal in diluted solutions. Additionally an offset ε is introduced to account for the deviation of measured data from theory as in [1], [6], [12]. Lastly, replacing activity with the molar concentration c_i changes the Nernst equation for VRFB to

$$E_{OCV} = E^0_C - E^0_A + RT/F \ln[c_{V5}\, c_{V2}/(c_{V4}\, c_{V3})] + \varepsilon \quad (3)$$

where R is the universal gas constant, T the temperature and F the Faraday constant. E^0_C and E^0_A are both temperature dependent

$$E^0_K(T) = E^0_{K,ref} + (dE/dT)_{K,ref}\,(T - T_{ref}) \quad (4)$$

Where $E^0_{K,Tref}$ is standard electrode potential of the half-reaction and $(dE/dT)_{K,ref}$ is its derivation with respect to temperature, both at reference temperature T_{ref} (here 298.15 K). K stands for either cathode or anode. In the following only one fitting parameter $(dE/dT)_{ref}$ will be used, which is the sum of the two respective values for cathode and anode reaction. As described above, the initial concentrations of the Vanadium ions c^0_V in catholyte and anolyte are equal and can be expressed through the state of charge:

$$c_{V2} = c_{V5} = SOC\, c^0_V \quad (5)$$

$$c_{V3} = c_{V4} = (1 - SOC)\, c^0_V \quad (6)$$

Substituting for concentrations in (3) gives

$$E_{OCV} = E^0 + 2RT/F \ln[SOC/(1\text{-}SOC)] + \varepsilon = E^0_{ref} + (dE/dT)_{ref}\,(T - T_{ref}) + 2RT/F \ln[SOC/(1\text{-}SOC)] + \varepsilon \quad (7)$$

Reference [8] suggest that the Nernst equation should also include the proton concentration at the cathode $c_{H,C}$, which changes proportionally with *V5* [5] and therefore

$$c_{H,C} = c^0_{H,C} + SOC\, c^0_V = c^0_V\,(H2V_C + SOC) \quad (8)$$

where $c^0_{H,C}$ is the initial concentration of protons in the catholyte and $H2V_C$ is the ratio of initial proton concentration to initial Vanadium ion concentration. Please note that the term initial refers to a SOC of zero and not the raw condition before pre-charging as described above. Including proton concentration rewrites (7) as

$$E_{OCV} = E^0_{ref} + (dE/dT)_{ref}\,(T - T_{ref}) + 2RT/F \ln[SOC\,(H2V_C + SOC) / (1 - SOC)] + \varepsilon \quad (9)$$

The initial Vanadium concentration as a factor in the final term of (8) will be dropped so it does not appear in the logarithm of (9) but it is rather included in the two fitting parameters $(dE/dT)_{ref}$ and ε.

3) Overpotentials

While OCV describes the reversible potential of a redox reaction, overpotentials η are attributed to losses associated with charge or mass transport. η is positive during charge and negative during discharge.

$$E_{cell} = E_{OCV} + \eta \quad (10)$$

where E_{cell} is the potential difference between the two poles of a cell. In this study, three types of overpotential are considered: ohmic, activation and concentration overpotential.

4) Resistance or ohmic overpotential

Ohmic overpotential η_{ohm} accounts for the electric resistivity in conductors such as current collector, membrane and electrolyte.

$$\eta_{ohm} = i\, \Sigma_j\, (h_j\, \rho_j) \quad (11)$$

where h and ρ are the thickness and the resistivity of conductor j and i is the current density defined as

$$i = I_{appl}/A_{cell} \quad (12)$$

where I_{appl} is the applied charging current of the cell and A_{cell} the geometrical cell area. The individual properties of the conductors are unknown, so an overall specific resistance of the cell r_{cell} is introduced in this study. This resistance is temperature dependent and, following a similar approach as [15], is described as

$$r_{cell} = \Sigma_j\, (h_j\, \rho_j) = r_{cell,ref} \exp[\, r\,(1/T - 1/T_{ref})] \quad (13)$$

where $r_{cell,ref}$ is the specific cell resistance at reference temperature and r is a fitting parameter describing the temperature sensibility of r_{cell}. To help understand (13) it should be noted that r_{cell} decreases with temperature in case of positive r and vice versa.

5) Activation overpotential

Electrochemical kinetics cause losses in redox reactions in form of activation overpotentials. Since this effect relates to electron exchange at electrode surface, the current density i_{el} used here differs from that in (12) as it is defined with respect to the active surface area of the porous electrodes A_{el} and not the cell area [2]

$$i_{el} = I_{appl} / A_{el} = I_{appl}/(A_{cell} a h_{el}) = i/(a h_{el}) \quad (14)$$

where a is the specific area of the cathode and h_{el} its thickness. The Butler-Volmer equation relates the current density to overpotentials and, when solved assuming identical charge transfer coefficients, gives

$$\eta_{act,C} = 2RT/F \operatorname{arsinh}\{i_{el}/[2Fk_C c^0_V (\mathrm{SOC}(1-\mathrm{SOC}))^{0.5}]\} \quad (15)$$

$$\eta_{act,A} = -2RT/F \operatorname{arsinh}\{i_{el}/[2Fk_A c^0_V (\mathrm{SOC}(1-\mathrm{SOC}))^{0.5}]\} \quad (16)$$

where $\eta_{act,K}$ and k_K are the activation overpotential and reaction rate constants associated with the cathode and anode reactions. The latter are functions of the temperature as described by [1]

$$k_K = k_{K,ref} \exp[F |E^0_{K,ref}| (1/T_{ref} - 1/T)/R] \quad (17)$$

where $k_{K,ref}$ is the reaction rate at reference temperature and K either cathode or anode.

6) Concentration overpotential

Concentration overpotentials account for limitations induced by mass transport effects, mainly the diffusion of Vanadium ions in the boundary layer formed around the electrode surface. Reference [12] state that the concentration overpotentials can be derived from the Nernst and Butler-Volmer equation when integrating concentration gradients that form due to the dynamics of mass transport. In the case of the Nernst equation [12] formulate

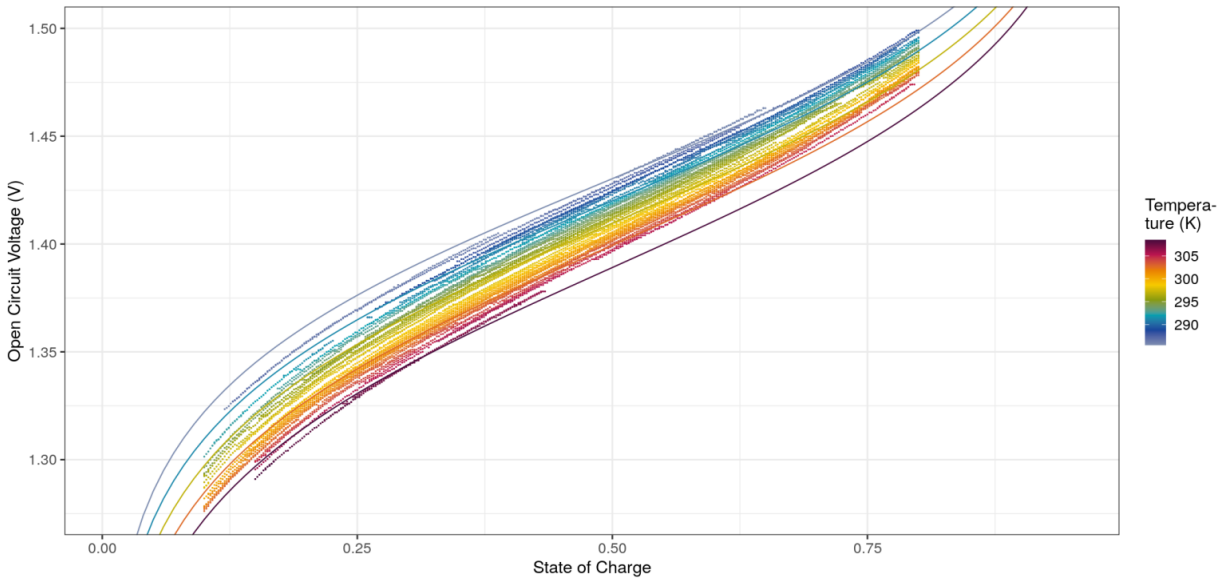

Fig. 1. Comparison of OCV simulation (lines) vs. experimental data (dots) without including proton concentration

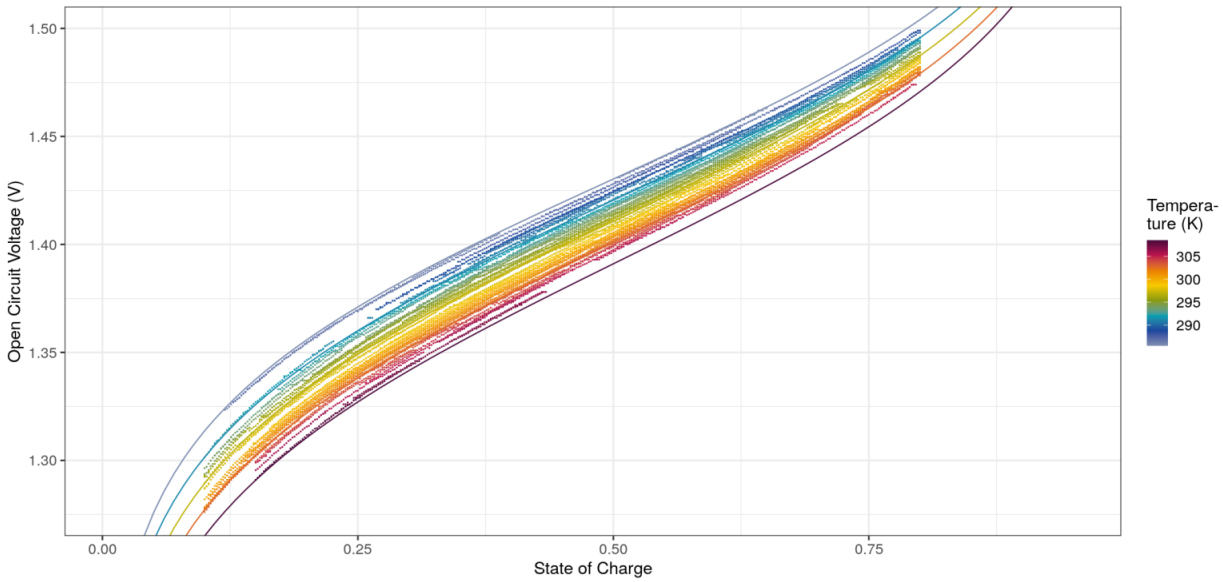

Fig. 2. Comparison of OCV simulation (lines) vs. experimental data (dots) including proton concentration

$$\eta_{conc,C}^{Nernst} = RT/F \ln[(1+\Delta c_{V5}/c_{V5}) / (1-\Delta c_{V4}/c_{V4})] \quad (18)$$

$$\eta_{conc,A}^{Nernst} = -RT/F \ln[(1+\Delta c_{V2}/c_{V2}) / (1-\Delta c_{V3}/c_{V3})] \quad (19)$$

where Δc_i is difference between the Vanadium ion concentration in the bulk electrolyte c_i and at the electrode surface c_i^S for species i. Δc_i is a function of the current density and the respective mass transport coefficient $k_{m,i}$.

$$\Delta c_i = c_i - c_i^S = i_{el} / (F\, k_{m,i}) \quad (20)$$

The latter can be estimated via the superficial velocity of the electrolyte v, a reference mass transport coefficient and another fitting parameter b:

$$k_{m,i} = k_{m,i,ref}\, v^b \quad (21)$$

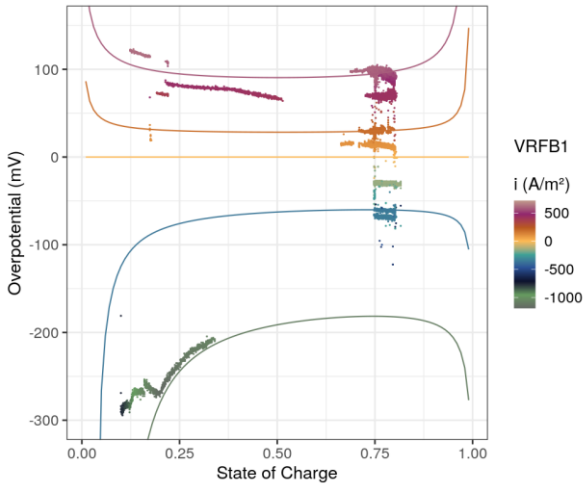

Fig. 3. Simulation (lines) vs. experimental data (dots) for 1st battery, only observations with T = (300±5 K) displayed

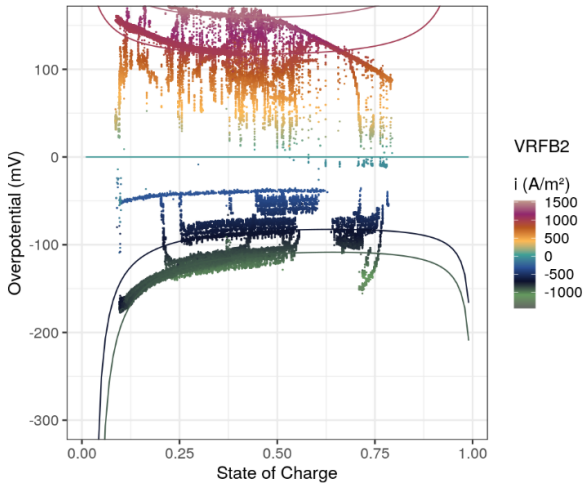

Fig. 4. Simulation (lines) vs. experimental data (dots) for 2nd battery, only observations with T = (302±1 K) displayed

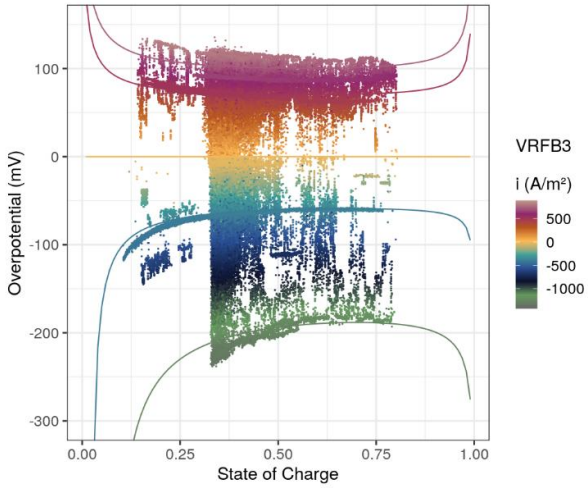

Fig. 5. Simulation (lines) vs. experimental data (dots) for 3rd battery, only observations with T = (302±1 K) displayed

The velocity inside the electrode is unknown but estimated with a pumping power P relation based on a simplistic approach derived from [18]:

$$v = 8\text{E-}3\ \text{ms}^{-1}\text{W}^{-1/3}\ P^{1/3} \qquad (22)$$

where the factor 8E-3 $\text{ms}^{-1}\text{W}^{-1/3}$ is an estimation based on cell geometry and undisclosed information from the manufacturer. To improve readability we introduce A, B, C and D for the $(1\text{-}\Delta c_i/c_i)$ terms (with i being $V2$, $V3$, $V4$ and $V5$) inside the logarithm of (18) and (19) and rewrite

$$\eta_{conc}^{Nernst} = \eta_{conc,C}^{Nernst} - \eta_{conc,A}^{Nernst} = RT/F \ln \frac{AD}{BC} \qquad (23)$$

Note that A and D are similar with respect to the plus sign as well as the fact that their bulk concentration relates to SOC. Whereas B and C include a minus sign and their bulk concentrations relate to (1–SOC). Concentration overpotential also stems from the Butler-Volmer equation but differs from charge to discharge [12]

$$\eta_{conc,cha}^{BV} = RT/F \ln 1/(B^2C^2) \qquad (24)$$

$$\eta_{conc,dis}^{BV} = RT/F \ln (A^2D^2) \qquad (25)$$

which finally leads to

$$\eta_{conc,cha} = RT/F \ln \text{AD}/(B^3C^3) \qquad (26)$$

$$\eta_{conc,dis} = RT/F \ln (A^3D^3)/\text{BC} \qquad (27)$$

III. Results and Discussion

A. Open Circuit Voltage

The fitting of the OCV is done without (7) and with (9) considering proton concentration. Additionally, (9) is adapted to include the Donnan potential as proposed by [11]

$$E_{\text{OCV}} = E^0_{\text{ref}} + (dE/dT)_{ref}\,(T - T_{ref}) + \varepsilon + RT/F \ln\{\text{SOC}^2(\text{H2V}_C + \text{SOC})^3/[(1 - \text{SOC})^2(\text{H2V}_A + \text{SOC})]\} \qquad (28)$$

which incorporates a second proton to Vanadium ratio H2V_A for the anode. The results for the fitted parameters and the root mean squared deviation can be found in table 1. Including proton concentration (9) reduces the error of the fit by 85 % in comparison to (7), while the inclusion of the Donnan potential further improves the fit by less than a permille. Additionally, a comparison of simulation results and experimental data can be found in Fig. 1 for (7) and Fig. 2 for (9). No separate diagram was created for (28) as there is no visual difference to Fig. 2. Equation (7) adequately represents the width of the range in OCV due to

temperature differences. This is achieved by including $(dE/dT)_{ref}$ in the Nernst equation. If it is not considered, all isothermal lines in a plot like Fig. 1 or Fig. 2 would intersect in one point with OCV = E^0_{ref} + ε and the SOC for which the term inside the logarithm is unity. Visually, (9) improves the fit by adjusting the slope of the isothermal lines. The values for ε lie within the range found in literature (131 mV [1], 124.5 mV [6], 155 mV [12]) while tendentially being lower when proton concentration is included. Experiments in the literature determining $(dE/dT)_{ref}$ select a SOC where the term inside the Nernst logarithm is unity and then measure the influence of temperature at this SOC: deriving -1.62 mV/K at 20 % SOC in [8] and -1.22 mV/K at 13.3 % SOC in [9]. Here, using the fitted value for $H2V_C$ of 2.024 in (9), the corresponding SOC value would be 30.1 %. [8] also measure $(dE/dT)_{ref}$ calorimetrically with -1.745 mV/K and another value can be found in [4] with -2.4 mV/K although the latter is partly estimated.

TABLE I. FITTED PARAMETERS AND ERROR FOR OCV VARIANTS

Eq.	$(dE/dT)_{ref}$	ε	$H2V_C$	$H2V_A$	RMSE
(7)	-1.791 mV/K	151.6 mV	-	-	3.858E-3
(9)	-1.866 mV/K	105.1 mV	2.024	-	5.608E-4
(28)	-1.861 mV/K	106.6 mV	1.676	1.211	5.607E-4

The SOC used in the fitting algorithm is not directly measured but a value that each battery estimates based on an undisclosed algorithm. The results presented here should therefore be interpreted as a form of reverse engineering of the relations implemented by the manufacturer and not a correct physical and electrochemical representation. Nevertheless, the derived model could be evaluated when transferred and applied on other experiments but therefore information on proton and Vanadium concentrations in the electrolyte used in this study would be necessary.

B. Overpotentials

The fitting algorithm for the overpotentials determines the specific cell resistance $r_{cell,ref}$ and its temperature dependency r, the reaction rates $k_{C,ref}$ and $k_{A,ref}$ and the power of the electrolyte velocity b. The terms A and D only differ in the mass transport coefficient $k_{m,ref,V2}$ and $k_{m,ref,V5}$ so the fitting algorithm cannot determine individual values for these. Therefore, one average value $k_{m,prod}$ is introduced as reference value for the products $V2$ and $V5$ and in an analogue manner $k_{m,react}$ for the reactants $V3$ and $V4$ so that term A equals D and B equals C. The seven fitting parameters are determined for each stack individually. With so many parameters to fit, selecting starting values as well as lower and upper limits requires a lot of iterations and finetuning. For several stacks only a solution could be found that run either into the upper or lower limit for one or more parameters. These cases are discarded and median values for the remaining stacks summarised in Table 2. As the outcome of a parameter in the fitting strongly influences the others and no stack reaches a close similarity with all medians from Table 2, a representative set of parameters for each battery is given in Table 3.

Reference values from literature are:

- for $k_{C,ref}$ in m/s: 3 E-9 [1]&[7], 6.4 E-8 [12], 6.8 E-7 [19]&[20]
- for $k_{A,ref}$ in m/s: 1.75 E-7 [1]&[7], 7.9 E-8 [12], 1.7 E-7 [17]&[20]
- most studies do not distinguish between different mass transfer coefficients and state for the k_m relation in (21): 1E-4 $v^{0.9}$ [12], 1.6E-4 $v^{0.4}$ [14]&[20], 1.3E-5 $v^{0.72}$ [10]&[20] (however the latter is a zinc-bromine system)

TABLE II. MEDIANS OF FITTED PARAMETERS FOR OVERPOTENTIALS

Parameter	Median
$r_{cell,ref}$	1.127 E-4 Ωm²
r	8.878 E2 K
$k_{C,ref}$	1.396 E-7 m/s
$k_{A,ref}$	4.268 E-8 m/s
b	1.277
$k_{m,prod}$	1.650 E-5 m/s
$k_{m,react}$	1.403 E-4 m/s

Reaction rates are in good compliance with literature while fitted mass transport coefficients tend to be smaller. Since the electrolyte flow velocity is expected to be way lower than 1 m/s, the generally higher values in this study for b would further decrease the whole expression in (21). Naturally, k_m and b have to be seen in context with (22). Any imprecision in the underlying power to flow relation of $P \sim Q^3$ is expressed in the fitted value for b. Fig. 3 to 5 display the comparison of simulation results based on the values from Table 3 and experimental data.

TABLE III. EXEMPLARY SETS OF FITTED PARAMETERS

Parameter	VRFB1	VRFB2	VRFB3
$r_{cell,ref}$/Ωm²	1.300 E-4	9.375 E-5	1.146 E-4
r/K	8.618 E2	1.576 E3	8.361 E2
$k_{C,ref}$/(m/s)	9.593 E-8	1.817 E-7	1.058 E-7
$k_{A,ref}$/(m/s)	2.892 E-7	5.052 E-8	4.205 E-8
b	1.776	1.338	8.637 E-1
$k_{m,prod}$/(m/s)	7.424 E-5	2.728 E-5	4.992 E-6
$k_{m,react}$/(m/s)	2.648 E-4	5.584 E-5	8.397 E-5

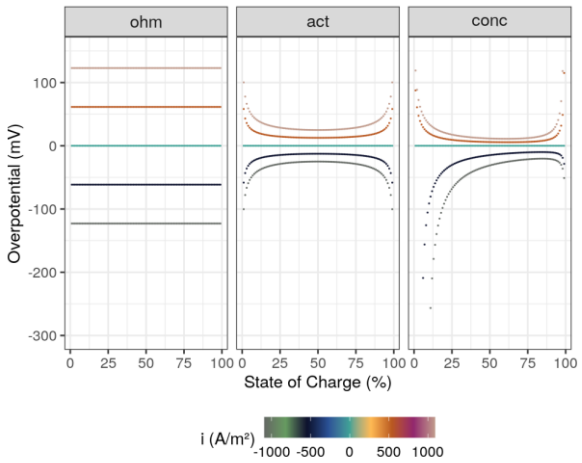

Fig. 6. Simulation of the different overpotential fractions for different SOC and current densities at 298 K, parameters are medians from Table 2

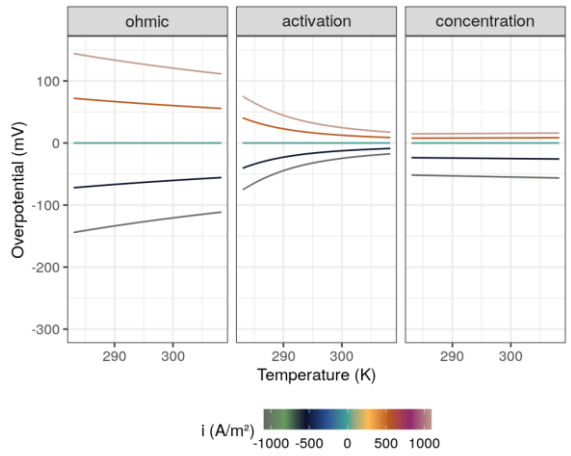

Fig. 7. Simulation of the different overpotential fractions for different temperatures and current densities at a SOC of 30 %, parameters are medians from Table 2

To put the different overpotential fractions into visual relation, simulated isocurrent lines are plotted in Fig. 6 and 7. Ohmic overvoltages have the biggest share, activation only coming close at low temperatures and concentration at extreme SOC levels, especially when discharging.

IV. Outlook

The influence of temperature on open circuit voltage and overpotentials is relevant (Fig. 7) but often neglected. The dependencies derived here vary from stack to stack and if temperature relations are depicted correctly is still an open question. For example, if the mass transfer coefficients are also a function of the temperature is an open questions. A respective parameter has been added to the fitting algorithm but it resulted in no further improvement or complicated the fitting by constantly running into limits. Although trying to formulate relations in a general matter, some of the assumptions like (22) are highly system specific. Further insight into key design attributes and additional measurements or separate experiments could help achieving more transferable parameters. Nevertheless, sound models of OCV and overpotentials like those presented here will be the basis of researching the remaining battery losses like shunt currents and auxiliary consumers.

Funded within SINTEG by the German Federal Ministry for Economic Affairs and Energy (BMWi) under 03SIN130

Acknowledgment

The research of this study was funded within the Smart Energy Showcases SINTEG by the German Federal Ministry for Economic Affairs and Energy (BMWi) as part of the project C/sells.

References

[1] H. Al-Fetlawi, A. A. Shah, und F. C. Walsh, „Non-isothermal modelling of the all-vanadium redox flow battery“, *Electrochimica Acta*, Bd. 55, Nr. 1, S. 78–89, Dez. 2009, doi: 10.1016/j.electacta.2009.08.009.

[2] I. M. Bayanov und R. Vanhaelst, „The numerical simulation of vanadium RedOx flow batteries“, *J Math Chem*, Bd. 49, Nr. 9, S. 2013–2031, Okt. 2011, doi: 10.1007/s10910-011-9872-x.

[3] C. Blanc und A. Rufer, „Multiphysics and energetic modeling of a vanadium redox flow battery“, in *2008 IEEE International Conference on Sustainable Energy Technologies*, Nov. 2008, S. 696–701, doi: 10.1109/ICSET.2008.4747096.

[4] S. G. Bratsch, „Standard Electrode Potentials and Temperature Coefficients in Water at 298.15 K“, *Journal of Physical and Chemical Reference Data*, Bd. 18, Nr. 1, S. 1, 1989, doi: 10.1063/1.555839.

[5] S. Corcuera und M. Skyllas-Kazacos, „State-of-Charge Monitoring and Electrolyte Rebalancing Methods for the Vanadium Redox Flow Battery“, *European Chemical Bulletin*, Bd. 1, Nr. 12, Art. Nr. 12, Nov. 2012, doi: 10.17628/ecb.2012.1.511-519.

[6] H. Fink, „Untersuchung von Verlustmechanismen in Vanadium-Flussbatterien“, TUM, München, 2019.

[7] M. Gattrell, J. Park, B. MacDougall, J. Apte, S. McCarthy, und C. W. Wu, „Study of the Mechanism of the Vanadium 4+/5+ Redox Reaction in Acidic Solutions“, *J. Electrochem. Soc.*, Bd. 151, Nr. 1, S. A123, Dez. 2003, doi: 10.1149/1.1630594.

[8] A. Heintz und C. Illenberger, „Thermodynamics of Vanadium Redox Flow Batteries - Electrochemical and Calorimetric Investigations“, *Berichte der Bunsengesellschaft für physikalische Chemie*, Bd. 102, Nr. 10, S. 1401–1409, 1998, doi: 10.1002/bbpc.199800009.

[9] N. S. Hudak, „Practical thermodynamic quantities for aqueous vanadium- and iron-based flow batteries“, *Journal of Power Sources*, Bd. 269, S. 962–974, Dez. 2014, doi: 10.1016/j.jpowsour.2013.12.089.

[10] K. Kinoshita und S. C. Leach, „Mass-Transfer Study of Carbon Felt, Flow-Through Electrode“, *J. Electrochem. Soc.*, Bd. 129, Nr. 9, S. 1993, Sep. 1982, doi: 10.1149/1.2124338.

[11] K. W. Knehr und E. C. Kumbur, „Open circuit voltage of vanadium redox flow batteries: Discrepancy between models and experiments“, *Electrochemistry Communications*, Bd. 13, Nr. 4, S. 342–345, Apr. 2011, doi: 10.1016/j.elecom.2011.01.020.

[12] S. K. Murthy, A. K. Sharma, C. Choo, und E. Birgersson, „Analysis of Concentration Overpotential in an All-Vanadium Redox Flow Battery“, *J. Electrochem. Soc.*, Bd. 165, Nr. 9, S. A1746, Juni 2018, doi: 10.1149/2.0681809jes.

[13] M. Pavelka, F. Wandschneider, und P. Mazur, „Thermodynamic derivation of open circuit voltage in vanadium redox flow batteries“, *Journal of Power Sources*, Bd. 293, S. 400–408, Okt. 2015, doi: 10.1016/j.jpowsour.2015.05.049.

[14] D. Schmal, J. Van Erkel, und P. J. Van Duin, „Mass transfer at carbon fibre electrodes“, *Journal of applied electrochemistry*, Bd. 16, Nr. 3, S. 422–430, 1986.

[15] A. A. Shah, R. Tangirala, R. Singh, R. G. A. Wills, und F. C. Walsh, „A Dynamic Unit Cell Model for the All-Vanadium Flow Battery“, *J. Electrochem. Soc.*, Bd. 158, Nr. 6, S. A671, Apr. 2011, doi: 10.1149/1.3561426.

[16] A. K. Sharma, C. Y. Ling, E. Birgersson, M. Vynnycky, und M. Han, „Verified reduction of dimensionality for an all-vanadium redox flow battery model“, *Journal of Power Sources*, Bd. 279, S. 345–350, Apr. 2015, doi: 10.1016/j.jpowsour.2015.01.019.

[17] E. Sum und M. Skyllas-Kazacos, „A study of the V(II)/V(III) redox couple for redox flow cell applications“, *Journal of Power Sources*, Bd. 15, Nr. 2, S. 179–190, Juni 1985, doi: 10.1016/0378-7753(85)80071-9.

[18] B. Xiong, J. Zhao, K. J. Tseng, M. Skyllas-Kazacos, T. M. Lim, und Y. Zhang, „Thermal hydraulic behavior and efficiency analysis of an all-vanadium redox flow battery“, *Journal of Power Sources*, Bd. 242, S. 314–324, Nov. 2013, doi: 10.1016/j.jpowsour.2013.05.092.

[19] T. Yamamura, N. Watanabe, T. Yano, und Y. Shiokawa, „Electron-Transfer Kinetics of Np3 +/Np4 + , NpO2 +/NpO2 2 + , V2 +/V3 + , and VO2 +/VO2 + at Carbon Electrodes“, *J. Electrochem. Soc.*, Bd. 152, Nr. 4, S. A830, März 2005, doi: 10.1149/1.1870794.

[20] D. You, H. Zhang, und J. Chen, „A simple model for the vanadium redox battery“, *Electrochimica Acta*, Bd. 54, Nr. 27, S. 6827–6836, Nov. 2009, doi: 10.1016/j.electacta.2009.06.086.